

# Near-Horizon Collisions around Near-Extremal Black Holes

Delilah E. A. Gates<sup>1,\*</sup>

<sup>1</sup>*Princeton Gravity Initiative, Princeton University, Princeton, New Jersey 08544, USA*

Black holes have sometimes been described as astrophysical particle accelerators because finite energy particles can collide near the horizon with divergent center-of-mass (CM) energy. The collisions are classified by the radial motion of the constituent particles at the moment of collision, with each class exhibiting a distinct near-horizon behavior. Divergence in the CM energy is sourced by the difference in the rate at which the collision radius approaches the horizon and the rate at which a particle's angular momentum is tuned to a critical value set by the superradiant bound. To produce a high energy collision around a near-extremal BH, at least one particle must approach criticality slower than the collision radius approaches the horizon. When both particles are ingoing or outgoing, it is additionally required that the particles approach criticality at different rates. Using a novel multi-scaling limit, we calculate the explicit form for the divergent CM energy.

## I. INTRODUCTION

A Kerr black hole (BH) can act as a particle accelerator allowing for collisions of divergent center-of-mass (CM) energy in the vicinity of the horizon. Such high energy collisions have been shown to occur if one particle has specific angular momentum taking on the critical value

$$L_* = \Omega_H^{-1} \mu \quad (1)$$

where  $\mu$  is the specific energy of the particle and  $\Omega_H$  is the angular velocity of the horizon, i.e., the particle is at the bound of superradiance. The existence of these high energy collisions was first identified by Bañados, Silk, and West, and is thus called the BSW-effect [1].

Explicit examples of high energy collisions between a critical particle and generic (non-critical) particle around a rapidly rotating BH have been worked out for two configurations: a pair of infalling particles colliding at the horizon, and an infalling generic particle colliding with a circular orbiter—wherein the orbiter is critical by virtue of having the angular momentum necessary to maintain its fixed radius close to the BH [2–6]. These examples exhibit CM energy which diverges as the BH tends to maximal spin, a feature intimately related to the special geometry of the near-extremal BH. In the rapidly rotating regime, the near-horizon region of a BH gets stretched into a throat-like geometry with proper radial depth which diverges as the BH approaches extremality [7]. The throat is described by the Near-Horizon Extremal Kerr (NHEK) metric and is the arena in which the high energy collisions take place [8].

In this paper, we take a careful look at near-horizon collisions around a near-extremal BH using a novel multi-scaling limit which tracks the rates at which we take 1) the collision radius to the horizon, 2) the colliding particles to criticality, and 3) the BH spin to extremality. This allows us to identify conditions under which the CM energy diverges, unifying previous results, and gives us new insight into their interpretation.

The outline is as follows: We start with a review of the CM energy of a pair of particles colliding around a sub-extremal Kerr BH where the near-horizon behavior of the CM energy can be classified by the radial motion of the constituent particles at the moment of collision (Sec. II). Next, we discuss the geometry of a near-extremal BH, develop the aforementioned multi-scaling limit, determine the conditions which lead to CM energy divergence, and calculate the explicit form of the CM energy. High energy collisions require at least one particle approaches criticality slower than the collision radius approaches the horizon—generic particles are included in this case—and, for pairs of ingoing or outgoing particles, the particles must approach criticality at different rates (Sec. III). We then specialize to high energy collisions which include a particle orbiting at or plunging from a circular orbit to contextualize the previous explicit examples, all which fall into this category (Sec. IV). Lastly, we provide a brief discussion of the naturalness and observability of these high energy collisions (Sec. V).

## II. HIGH ENERGY COLLISIONS AROUND SUB-EXTREMAL BHs

A rotating BH of mass  $M$  and angular momentum  $J = aM$  is described by the Kerr metric, which in Boyer-Lindquist (BL) coordinates is<sup>1</sup>

$$ds^2 = -\frac{\Delta}{\Sigma} (dt - a \sin^2 \theta d\phi)^2 + \frac{\Sigma}{\Delta} dr^2 + \Sigma d\theta^2 + \frac{\sin^2 \theta}{\Sigma} [(r^2 + a^2) d\phi - a dt]^2, \quad (2)$$

where  $\Delta = r^2 - 2Mr + a^2$  and  $\Sigma = r^2 + a^2 \cos^2 \theta$ . The event horizon is located at radius

$$r_H = M + \sqrt{M^2 - a^2}, \quad (3)$$

and has angular velocity  $\Omega_H = a/(2Mr_H)$ .

\* [deagates@princeton.edu](mailto:deagates@princeton.edu)

<sup>1</sup>We use natural units  $G_N = c = 1$ .

Timelike geodesics of particle motion in the Kerr geometry can be parameterized by four independent conserved quantities: the particle mass  $m$ , specific energy (energy per particle mass)  $\mu$ , specific azimuthal angular momentum  $L$ , and specific Carter constant  $Q$ . The momentum  $p$  of a geodesic particle is given by

$$\frac{p}{m} = -\mu dt + \bar{s}_r \frac{\sqrt{\mathcal{R}(r)}}{\Delta(r)} dr + \bar{s}_\theta \sqrt{\Theta(\theta)} d\theta + L d\phi \quad (4)$$

where the angular and radial potentials are

$$\Theta(\theta) = Q + a^2(\mu^2 - 1) \cos^2 \theta - L^2 \cot^2 \theta \quad (5)$$

$$\mathcal{R}(r) = P^2(r) - \Delta(r)T(r),$$

$$P(r) = \mu^2(r^2 + a^2) - aL,$$

$$T(r) = Q + (L - a\mu)^2 + r^2, \quad (6)$$

and where  $\bar{s}_r$  and  $\bar{s}_\theta$  are  $\pm 1$  when the respective potentials are non-zero, and are zero when the respective potentials are zero.

Let us consider the collision between two timelike geodesic particles. The CM energy of the collision is given in terms of the total momentum of the system  $p_{\text{tot}}^a = p_1^a + p_2^a$  as follows

$$E_{\text{cm}}^2 = -p_{\text{tot}} \cdot p_{\text{tot}} = m_1^2 + m_2^2 - 2p_1 \cdot p_2. \quad (7)$$

This quantity is given by

$$\frac{E_{\text{cm}}^2}{m_1 m_2} = \frac{m_1^2 + m_2^2}{m_1 m_2} + \frac{2(\chi - \mathcal{Y})}{\Sigma}, \quad (8)$$

$$\chi = \frac{P_1 P_2 - \bar{s}_{r_1} \bar{s}_{r_2} \sqrt{\mathcal{R}_1} \sqrt{\mathcal{R}_2}}{\Delta}, \quad (9)$$

$$\mathcal{Y} = \frac{(L_1 - \mu_1 a \sin^2 \theta)(L_2 - \mu_2 a \sin^2 \theta)}{\sin^2 \theta} + \bar{s}_{\theta_1} \bar{s}_{\theta_2} \sqrt{\Theta_1} \sqrt{\Theta_2}. \quad (10)$$

Now we will examine the near-horizon limit of the CM energy (8) in the sub-extremal case, and consider the implication of then taking the extremal limit. With the exception of the term containing  $\chi$ , all the terms of the CM energy (8) are clearly finite for all  $r \geq r_{\text{H}}$ . We evaluate the near-horizon limit of  $\chi$  in three distinct classes distinguished by the radial motion of the particles at the moment of collision. The classes are Type I in which one particle is outgoing and the other is ingoing, Type T in which one particle has no radial motion, and Type V in which both particles are either ingoing or outgoing; see Fig. 1. In the near-horizon limit  $r \rightarrow r_{\text{H}}$ ,

$$\chi_{\text{sub}} = \begin{cases} \frac{T_2(r_{\text{H}})\hat{L}_1}{2\hat{L}_2} + \frac{T_1(r_{\text{H}})\hat{L}_2}{2\hat{L}_1} + \mathcal{O}(r - r_{\text{H}}), & s_r = 1 \\ \frac{(1 - s_r)a^2\hat{L}_1\hat{L}_2}{2\sqrt{M^2 - a^2}(r - r_{\text{H}})} + \mathcal{O}(1), & s_r \leq 0 \end{cases}, \quad (11)$$

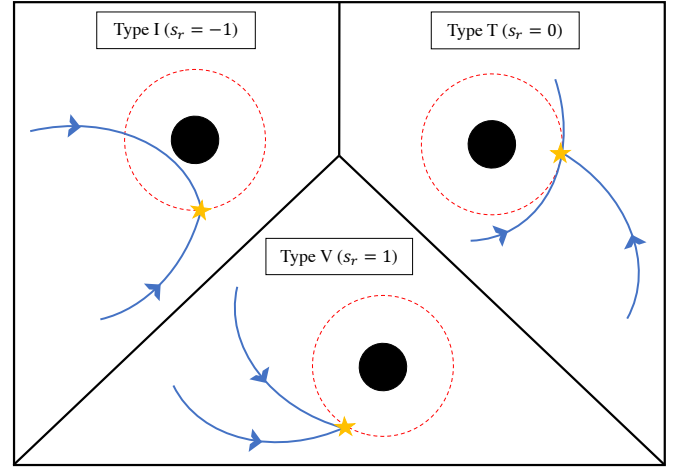


FIG. 1. Schematic depictions of particles colliding near BH. Collisions are categorized by the radial motion of particles at the moment of collision. The motion of the particles is shown in blue (with arrows for direction), collision location in yellow, collision radius in red, and the BH horizon in black.

where  $\hat{L}_i \equiv L_i - \Omega_{\text{H}}^{-1} \mu_i$ , and  $s_r \equiv \text{sgn}(\bar{s}_{r_1} \bar{s}_{r_2})$ . Necessarily we take  $\text{sgn}(\hat{L}_1) = \text{sgn}(\hat{L}_2)$  to maintain positivity<sup>2</sup>.

In Type V collisions, deviation of the collision radius from the horizon does not play a direct role in the divergence of the CM energy—the particles are not a priori at large boost to one another. In fact  $\chi(r = r_{\text{H}}, s_r = 1) = 0$ . By contrast, the CM energy of Type I and Type T collisions diverges near the horizon with the deviation of the collision radius from the horizon, as the particles are at parametrically large boost to one another.

Examining Eq. (11), it is evident that setting a particle to criticality (1) and/or taking the BH to extremality may change the divergence of the near-horizon CM energy. The critical angular momentum is related to the remarkable property of BH superradiance whereby an object with  $\mu \leq \Omega_{\text{H}} L$  can scatter off the BH with amplified energy. We note that some of these aspects about near-horizon high energy collisions are discussed in Ref. [9] by Harada and Kiumura (HK). Next we will work out, in detail, the form of the divergent CM energy for collisions which include critical particles.

### A. Collisions with critical particles

The divergent Type V collision between a generic and critical particle was first discovered by BSW in the extremal BH case. BSW examined a pair of ingoing particles originating far from the BH, traveling along geodesics, which collided at the horizon, the so-called

<sup>2</sup>Moving forward we will not explicitly mention the conditions needed to maintain positivity of the CM energy.

“direct collision scenario” [1]. (See App. A for treatment of the extremal case.) Subsequently, Grib and Pavlov (GP) showed the existence of the near-horizon high energy Type V collision for a sub-extremal BH. At sub-extremality a critical particle at infinity cannot reach the horizon along a geodesic. Such a collision requires a “multiple scattering” scenario in which one particle has its angular momentum critically tuned through other means, e.g., interacting with other particles in an accretion disk as it migrates towards the horizon or originating from a prior near-horizon scattering process [3, 4]<sup>3</sup>. Eq.(11) suggest that tuning a particle to criticality will affect the CM energy divergence of Type T and I collisions as well.

To take the near-horizon, near-critical limit, we set

$$r = r_{\text{H}} + M\epsilon, \quad 0 < \epsilon \ll 1, \quad (12a)$$

$$L_i = \Omega_{\text{H}}^{-1} \mu_i (1 - f_i), \quad 0 \leq n_i \quad (12b)$$

where  $f_i(n_i = 0) = \ell_i$  and  $f_i(n_i > 0) = \epsilon^{n_i}$ . The function  $f_i$  allows us to represent the limit with generic ( $n_i = 0$ ) and criticality tuned ( $n_i < 0$ ) particles. Rewriting (9) as

$$\chi = \tilde{P}_1 \tilde{P}_2 - s_r \sqrt{\tilde{P}_1^2 - T_1} \sqrt{\tilde{P}_2^2 - T_2}, \quad (13)$$

where  $\tilde{P} = P/\sqrt{\Delta}$ , the (possible) divergence of the CM energy can be diagnosed by examining  $\tilde{P}$  and  $T$ . To leading order in the limit  $\epsilon \rightarrow 0$ ,

$$\tilde{P}_i = \frac{\mu_i r_{\text{H}} \sqrt{2M\epsilon}}{(M^2 - a^2)^{1/4}} \begin{cases} 1 + \delta(n_i - 1), & n_i \geq 1 \\ \frac{1 + \ell_i \delta(n_i)}{\epsilon^{1-n_i}}, & 0 \leq n_i < 1 \end{cases}, \quad (14)$$

$$T_i = r_{\text{H}} + Q_i + \frac{\mu_i^2 r_{\text{H}}^2}{a^2} [r_{\text{H}} + 2M\ell_i \delta(n_i)]^2, \quad (15)$$

where  $\delta(x)$  is the Dirac delta function. Particle motion is only allowed when  $R_i \propto \tilde{P}_i^2 - T_i \geq 0$ .  $T_i$  is always finite and non-vanishing, so we must additionally restrict  $n_i \leq 1/2$  such that  $\tilde{P}_i$  is also non-vanishing.

To produce divergent CM energy,  $\tilde{P}_i$  of at least one particle must be divergent, i.e.,  $n_i < 1/2$ . When only one particle satisfies the divergence condition ( $n_1 < 1/2 = n_2$ ), which we will call “singly sourced divergence”,  $\chi$  to leading order is

$$\chi_{\text{sub}} = \tilde{P}_1 \tilde{P}_2 - s_r \sqrt{\tilde{P}_1^2} \sqrt{\tilde{P}_2^2 - T_2} \sim \frac{1}{\epsilon^{1/2-n_1}}, \quad (16)$$

which has a universal form for all collision Types. Alternatively, both particles may satisfy the divergence condition, which we will call “doubly sourced divergence”. Here the CM energy of Type I and T collisions is divergent when  $n_1 \leq n_2 < 1/2$ , where  $\chi$  to leading order is

$$\chi_{\text{sub}} = (1 - s_r) \tilde{P}_1 \tilde{P}_2 \sim \frac{1}{\epsilon^{1-n_2-n_1}}. \quad (17)$$

The CM energy of the Type V collision is only divergent when  $n_1 < n_2 < 1/2$ , where  $\chi$  to leading order is

$$\chi_{\text{sub}} = \frac{T_2 \tilde{P}_1}{2\tilde{P}_2} \sim \frac{1}{\epsilon^{n_2-n_1}}, \quad (18)$$

This is the expected form of divergent CM energy one could deduce from (11). Note high energy collisions of two critical particles are allowed for singly and doubly sourced collisions of all Types.

## B. Collisions in the extremal limit

As Eqs. (14)-(17) suggests, the divergence of the near-horizon CM energy is affected by deviation from maximal BH spin in the singly divergent collisions of all Types and doubly divergent Type I and T collisions. Explicit examples of high energy collisions between generic and critical particles around near-extremal BHs have been worked out. Type V collisions at the horizon which diverge as  $E_{\text{cm}} \sim (1 - a^2/M^2)^{-1/4}$  have been shown to exist numerically by Jacobson and Sotiriou (JS) and analytically by GP and by HK [2-6].

High energy Type T collisions of generic particles and circular orbiters have been shown to exist around near-extremal BHs. These circular orbiter collisions are only possible for a near-extremal BH as prograde circular orbits only become close to the horizon in the near-extremal limit. JS numerically showed that collisions with an orbiter at the prograde innermost bound circular orbit (IBCO) exhibit a  $E_{\text{cm}} \sim (1 - a^2/M^2)^{-1/4}$  divergence; while, HK analytically showed that collisions with an orbiter at the prograde innermost stable circular orbit (ISCO) exhibit a  $E_{\text{cm}} \sim (1 - a^2/M^2)^{-1/6}$  divergence [2, 5, 6]. In the extremal limit, the prograde IBCO and ISCO orbiters do have critically tuned angular momentum.

Fully resolving the behavior of near-horizon collisions around a near-extremal BH necessitates keeping track of the rates at which the collision radius approaches the horizon, the particles approach criticality (if they approach it at all), and the BH approaches extremality, but insights gleaned here will carry over to the near-extremal case. Firstly, high energy collisions require that at least one particle have angular momentum which scales to criticality sufficiently “slowly” compared to the rate the collision radius scales to the horizon, allowing for both singly and doubly divergent collisions. Type V collisions additionally require that the particles approach criticality at different rates. Secondly, the CM energy divergence of the singly divergent collisions of all Types and doubly divergent Type I and T collisions is set by the difference in rate at which the collision radius approaches the horizon and the rates at which particles approach criticality. The CM energy divergence of the doubly divergent Type V collision is set by the difference in rates at which the particles approach criticality. Next we will calculate the

<sup>3</sup>Particles with vanishing specific energy can also produce divergent near-horizon CM energy [10].

general form of the high energy CM energy for collisions around near-extremal BHs. The multi-scaling limit required to carry out this calculation is intimately linked to the geometry of the near-extremal BH.

### III. HIGH ENERGY COLLISIONS AROUND NEAR-EXTREMAL BH

A near-extremal BH can be described with small parameter  $\kappa = \sqrt{1 - a^2/M^2}$ , which sets the horizon at

$$r_H = M(1 + \kappa). \quad (19)$$

At extremality the horizon goes to  $r = M$ . However, in the extremal limit, several physically distinct radii such as the prograde photon circular orbit (PCO), IBCO, and ISCO radii also approach  $r = M$ . In actuality, as the BH spin is increased, the near-horizon region develops a throat-like geometry of proper radial depth which diverges with deviation from extremality  $\kappa$ . For this reason it is well known that BL coordinates do not resolve the near-horizon physics of near-extremal BHs [7].

To resolve the near-horizon physics, we examine the scaling rate of different BL radii near the extremal limit. Radii which scale as

$$r - M \sim \kappa^p, \quad 0 < p \leq 1 \quad (20)$$

in the extremal limit approach the horizon. Radii which scale with the same value of  $p$  maintain finite proper distance from one another in the extremal limit; radii which scale with different values of  $p$  have divergent proper distance in the extremal limit. All BL radii which scale with  $0 < p < 1$  are described by the limiting metric known as the near-horizon extreme Kerr (NHEK) metric. Radii which scale with  $p = 1$  are described by a different limiting metric, the near-NHEK [8, 11] (see App. B). On the other hand, radii that do not scale to  $r = M$ , such as the retrograde PCO, IBCO, and ISCO radii, remain in the far region of the geometry which is described by the extreme Kerr metric (given by (2) with  $a = M$ ).

Each set of radii with scaling  $r - M \sim \kappa^p$  is physically distinct. Radii which scale with the same power  $p$ , end up in the same NHEK and are said to exist in the same “ $p$ -band” of the near-extremal BH geometry. The horizon and prograde PCO and IBCO radii belong to the  $p = 1$  band (i.e. the near-NHEK) while the prograde ISCO radius belongs to the  $p = 2/3$  band. The far region can be thought of as the  $p = 0$  band. The full geometry of the near-extremal BH can be thought of as the ensemble of all the infinitely many  $p$ -bands (see Fig. 2). Any process which involves both the rate at which a radius approaches the horizon  $\kappa^p$  and the rate at which the BH spin increases  $\kappa$  must be calculated as a limit applied to the sub-extremal case [12].

We must also consider the rates at which particles approach criticality. As the BH spin approaches maximum,

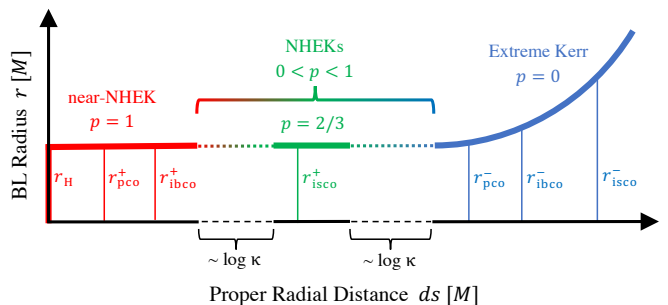


FIG. 2. Geometry of a near-extremal BH. In the near-extremal limit  $\kappa = \sqrt{1 - a^2/M^2} \ll 1$ , the Kerr BH develops a throat-like geometry of divergent proper depth. All radii which approach  $r = M$  at the same rate ( $r - M \sim \kappa^p$ ) as the BH approaches extremality are described by the same limiting metric (near-NHEK, NHEK, or extreme Kerr). The horizon and the prograde and retrograde PCO, IBCO, and ISCO radii are marked.

the critical angular momentum (1) goes as

$$L_* = \Omega_H^{-1} \mu = 2M\mu[1 + \kappa + \mathcal{O}(\kappa^2)], \quad (21)$$

which reaches  $L = 2M\mu$  at extremality. Particles whose angular momenta scale as

$$2M\mu - L \sim \kappa^q, \quad 0 < q \quad (22)$$

in the near extremal limit approach criticality; these include prograde PCO, IBCO, and ISCO orbiters. Generic particles, those with angular momenta which does not scale to criticality in the nextremal limit, include retrograde PCO, ISCO, and IBCO orbiters.

Therefore, we will consider the CM energy collisions in the Kerr background (8) under the multiple-scaling limit set by applying

$$a = M\sqrt{1 - \kappa^2}, \quad 0 < \kappa \ll 1, \quad (23a)$$

$$r = M(1 + R\kappa^{p_c}), \quad 0 < p_c < 1, \quad (23b)$$

$$L_i = 2M\mu_i(1 - l_i\kappa^{q_i}), \quad 0 \leq q_i. \quad (23c)$$

The radial parameter  $R$  and angular momenta parameter  $l_i$  are dimensionless. We use  $p_c$  to control the rate at which the BL collision radius scales to  $M$ , and  $p_i$  to control the rate at which the angular momenta of the particles scale to  $2M$ .

#### A. High energy collisions

When  $\chi$  (9) is divergent in the scaling limit defined in (23), the CM energy is

$$\frac{E_{\text{cm}}^2}{m_1 m_2} \approx \frac{2\chi_{\text{near}}}{M^2(1 + \cos^2 \theta)}. \quad (24)$$

As in the sub-extremal case, the (possible) divergence of the CM energy can be diagnosed by examining  $\dot{P}$  and  $T$

in the limit (23). To leading order in the scaling limit,

$$\tilde{P}_i = \frac{2M\mu_i}{\sqrt{R^2 - \sigma_c}} \begin{cases} R + l_i\delta(q_i - p_c), & q_i \geq p_c \\ \frac{l_i}{\kappa^{p_c - q_i}}, & q_i < p_c \end{cases}, \quad (25)$$

$$T_i = M^2 \left[ 1 + \eta_i + \mu_i^2 [1 + l_i\delta(q_i)]^2 \right], \quad (26)$$

where  $\sigma_j \equiv \delta(1 - p_j)$  is defined through the Dirac delta function, and where  $\eta_i = Q_i/M^2$  is the dimensionless Carter constant. As  $\tilde{P}_i$  is non-vanishing and  $T_i$  is non-vanishing and finite,  $R_i \propto \tilde{P}_i^2 - T_i \geq 0$  imposes no condition on  $q_i$  (in contrast to the sub-extremal case).

Divergent CM energy requires that at least one particle has angular momentum which scales to criticality slower than the collision radius scales to the horizon ( $p_i < p_c$ ). When only one particle satisfies this condition  $q_1 < p_c \leq q_2$ , singly sourced divergence,  $\chi$  to leading order becomes

$$\chi_{\text{near}} = \tilde{P}_1 \tilde{P}_2 - s_r \sqrt{\tilde{P}_1^2} \sqrt{\tilde{P}_2^2 - T_2} \sim \frac{1}{\kappa^{p_c - q_1}}. \quad (27)$$

When both particles satisfy the divergence condition, doubly sourced divergence, we examine the different particle types separately. For Type I and T collisions, the CM energy is divergent when  $q_1 \leq q_2 < p_c$ , and  $\chi$  takes the form

$$\chi_{\text{near}} = (1 - s_r) \tilde{P}_1 \tilde{P}_2 \sim \frac{1}{\kappa^{2p_c - q_2 - q_1}}, \quad (28)$$

in the scaling limit. For Type V collisions, the CM energy is only divergent when  $q_1 < q_2 < p_c$ , and  $\chi$  becomes

$$\chi_{\text{near}} = \frac{T_2 \tilde{P}_1}{2\tilde{P}_2} \sim \frac{1}{\kappa^{q_2 - q_1}}. \quad (29)$$

Further, we can bound the divergence rates of high energy collisions. Singly sourced divergence (27) is strongest when the collision takes part in the near-NHEK region ( $p_c = 1$ ) and particle 1 is generic ( $q_1 = 0$ ),

$$E_{\text{cm}} \sim \kappa^{-(p_c - q_1)/2} \leq (1 - a^2/M^2)^{-1/4}. \quad (30)$$

The doubly sourced divergent Type V collision (29) is subject to a similar constraint,

$$E_{\text{cm}} \sim \kappa^{-(q_2 - q_1)/2} < (1 - a^2/M^2)^{-1/4}. \quad (31)$$

On the other hand, the doubly sourced divergent Type I and T collision (28) diverges as

$$E_{\text{cm}} \sim \kappa^{-p_c + (q_2 + q_1)/2} < (1 - a^2/M^2)^{-1/2}. \quad (32)$$

#### IV. HIGH ENERGY COLLISIONS WITH CIRCULAR ORBIT PARTICLES

Several configurations leading to divergent CM energy collisions have been outlined in previous works. Explicit

examples have considered collisions between generic and critical particles which are bound to the equatorial plane ( $\theta = \pi/2$ ,  $p_\theta = 0$ ,  $Q = 0$ ). In said examples, the critical particle is a circular orbiter (a particle at the circular orbit radius  $r = r_o$  with specific energy and angular momentum needed to maintain fixed radius  $\mu = \mu_o(r_o)$  and  $L = L_o(r_o)$ ) or a plunging particle with the specific energy and angular momentum of a circular orbiter  $\mu = \mu_o(r_o)$  and  $L = L_o(r_o)$  but at radii  $r < r_o$ ; and, the generic particle is either a circular orbit particle or marginally bound zero angular momentum particle (MBZAM) for which  $\mu = 1$  and  $L = 0$ . The collisions have been shown to take place at the horizon and the prograde IBCO and ISCO radii.

##### A. Circular orbit particles in the near-horizon, near-critical limit

Massive circular orbiters in the Kerr geometry (2), defined by  $\mathcal{R}(r_o) = \mathcal{R}'(r_o) = 0$ , have specific energy and angular momentum [7]

$$\mu_o^\pm = \frac{r_o^{3/2} - 2M\sqrt{r_o} \pm a\sqrt{M}}{\sqrt{r_o^3 - 3Mr_o^2 \pm 2a\sqrt{M}r_o^{3/2}}}, \quad (33a)$$

$$L_o^\pm = \pm\mu_o^\pm \frac{\sqrt{M}(r_o^2 + a^2) \mp 2aM\sqrt{r_o}}{\sqrt{r_o^3 - 3Mr_o^2 \pm 2a\sqrt{M}r_o^{3/2}}}, \quad (33b)$$

with prograde/retrograde denoted by the  $\pm$ . These orbits exist outside of radius of the PCO

$$r_{\text{pco}}^\pm = 2M \left[ 1 + \cos \left[ \frac{2}{3} \arccos \left( \mp \frac{a}{M} \right) \right] \right], \quad (34)$$

where the denominator of the specific energy goes to zero. Bound ( $\mu \leq 1$ ) circular orbiters exist at radii down to the IBCO $^\pm$  radius

$$r_{\text{ibco}}^\pm = 2M \mp a + 2\sqrt{M(M \mp a)}, \quad (35)$$

where the angular momentum reduces to the simple form  $L_{\text{ibco}}^\pm = \pm \left[ M + \sqrt{M(M \mp a)} \right]$ . Circular orbits are stable  $\mathcal{R}''(r_o) < 0$  down to the ISCO $^\pm$  radius

$$r_{\text{isco}}^\pm = M \left[ 3 + Z_2 \mp \sqrt{(3 - Z_1)(3 + Z_1 + 2Z_2)} \right], \quad (36a)$$

$$Z_1 = 1 + \sqrt[3]{1 - \frac{a^2}{M^2}} \left( \sqrt[3]{1 + \frac{a}{M}} + \sqrt[3]{1 - \frac{a}{M}} \right), \quad (36b)$$

$$Z_2 = \sqrt[3]{3 \frac{a^2}{M^2} + Z_1^2}. \quad (36c)$$

Outside the equatorial plane there are spherical orbits of fixed radii which are stable down to the last stable spherical orbit (LSSO), and which are bound down to the last spherical bound orbit (LBSO); although, no closed form description of these non-equatorial spherical



orbits exist [13–15]. In the extremal limit, LBSO and LSSO radii which scale to  $r = M$  exist only within latitudes  $\pm \arccos(2/3)$  and  $\pm \arccos(\sqrt{3} - 1)$ , respectively; and thus, high energy collisions which include LSSO and LBSO particles exist only within the respective latitude bands [6, 13].

We will consider collisions which include particles on circular orbits and the associated particles which have the same conserved quantities as a circular orbiter and plunge towards the horizon. A plunging particle associated with a stable circular orbiter ( $\mu = \mu_o(r_o), L = L_o(r_o), r_o > r_{\text{isco}}$ ) cannot be thought of as plunging *from* the circular orbiter radius  $r_o$ ; instead it travels along a geodesic which begins and ends on the horizon and has a radial turning point strictly less than  $r_o$ . By contrast, a plunger associated with the ISCO or an unstable circular orbiter ( $r_o \leq r_{\text{isco}}$ ) travels along a geodesic which asymptotically spirals out of the circular orbit radius and plunges into the horizon. These plungers can be thought of as plunging from the circular orbit radius [16].

Additionally we note, a particle with the conserved quantities of an unstable circular orbiter can asymptotically spiral onto or out of the circular orbit radius [16, 17]. Previous works by JS and HK (Refs. [2, 5, 6]) consider collisions between a generic particle and an infalling critical particle, with  $\mu = 1$  and  $L_{\text{ibco}}^+$ , that occurs on the IBCO<sup>+</sup> radius. As the IBCO<sup>+</sup> orbiter is the limiting particle of the critical particle in these collisions, they are effectively Type T collisions with an IBCO<sup>+</sup> orbiter.

To calculate the CM energy of a high energy collision, we need the radial parameter  $R$  and scaling value  $p$  of the collision radius, By (23b), the near-extremal limit  $R\kappa^p \approx r - M$  provides the parameters. These parameters of the ISCO<sup>±</sup> radii, IBCO<sup>±</sup> radii, and horizon are provided in Table I (left side). As the all retrograde radii remains in the asymptotically far region of the near-extremal BH geometry  $q = 0$ , high energy collisions cannot occur at the retrograde circular orbit radii. However, the IBCO<sup>+</sup> radius exists in the  $p = 1$  band, so prograde circular orbiters can exist in all  $p$ -bands and high energy collisions can occur at any prograde circular orbit radii in the throat.

We also need the specific energy  $\mu$  and angular momentum parameter  $l$  and scaling value  $q$  of each participating particle. By (23c), the near-extremal limit  $l\kappa^q \approx 1 - L/(2M\mu)$  provides the latter of these. Both ISCO<sup>+</sup> and IBCO<sup>+</sup> orbiters have critically tuned angular momentum. The specific energy, angular parameters  $l$ , and scaling values  $q$  for IBCO<sup>±</sup>, ISCO<sup>±</sup> orbiters and MBZAMs are shown in Table I (right side).

We can also consider a circular orbiter (33) at a general near-horizon radius  $r_o = M(1 + R_o\kappa^{p_o})$  with  $0 < p_o \leq 1$ . In the near-extreme limit  $\kappa \ll 1$ , the circular orbiter has specific energy

$$\mu_o = \frac{R_o}{\sqrt{3R_o^2 - 4\sigma_o}}, \quad (37)$$

Radius	$R$	$p$	Particle Type	$\mu$	$l$	$q$
ISCO <sup>+</sup>	$2^{1/3}$	$\frac{2}{3}$	ISCO <sup>+</sup> orbiter	$\frac{1}{\sqrt{3}}$	$-\frac{3}{2^{4/3}}$	$\frac{4}{3}$
IBCO <sup>+</sup>	$\sqrt{2}$	1	IBCO <sup>+</sup> orbiter	1	$-\frac{1}{\sqrt{2}}$	1
ISCO <sup>-</sup>	8	0	ISCO <sup>-</sup> orbiter	$\frac{5}{3^{3/2}}$	$\frac{16}{5}$	0
IBCO <sup>-</sup>	$2(1 + \sqrt{2})$	0	IBCO <sup>-</sup> orbiter	1	$2 + \sqrt{2}$	0
horizon	1	1	MBZAM	1	1	0

TABLE I. Left: radial parameter  $R$  and scaling value  $p$  of various BL radii. Right: specific energy  $\mu$ , angular momentum parameter  $l$ , and scaling value  $q$  of various particles.

and angular momentum parameter and scaling value

$$q_o = \min(2p_o, 2 - p_o), \quad (38)$$

$$l_o = \begin{cases} -\frac{R_o}{4}, & 0 < p_o < \frac{2}{3} \\ -\frac{R_o^2 + 4}{4R_o}, & p_o = \frac{2}{3} \\ -\frac{1}{R_o}, & \frac{2}{3} < p_o \leq 1 \end{cases}. \quad (39)$$

As  $q_o > 0$ , near-horizon circular orbiters are naturally tuned to criticality, and circular orbit plungers can source divergence in high energy collisions.

## B. Type T Collisions with circular orbiters

Here we examine Type T collisions which include a circular orbiter. By (38)  $p_o \leq q_o$ , so Type T collisions with circular orbiters ( $p_c = p_o$  and  $q_2 = q_o$ ) can only exhibit singly sourced divergences (27). The CM energy for a circular orbiter collisions is thus given by

$$\frac{E_{\text{cm}}^2}{m_1 m_2} = \frac{8\mu_1 l_1}{\sqrt{3R_o^2 - 4\sigma_c \kappa^{p_c - q_1}}}. \quad (40)$$

The strongest CM energy divergence occurs when the circular orbiter is in the near-NHEK band ( $p_c = 1$ ) and the ingoing particle is generic ( $q_1 = 0$ ). In general, we find the CM energy between a generic particle and circular orbiter diverges in relation to the  $p$ -band in which the orbiter resides,

$$E_{\text{cm}} \sim \kappa^{-p_c/2} = (1 - a^2/M^2)^{-p_c/4}, \quad (41)$$

explaining the CM energy divergence seen in previously studied collisions with ISCO<sup>+</sup> and IBCO<sup>+</sup> orbiters. When the orbiter is at the ISCO<sup>+</sup> or IBCO<sup>+</sup> radius, the CM energy is

$$\frac{E_{\text{cm}}^2}{m_1 m_2} = 4\mu_1 l_1 \begin{cases} \frac{2^{2/3}}{\sqrt{3}\kappa^{2/3}}, & \text{ISCO}^+ \text{ orbiter} \\ \frac{2^{1/2}}{\kappa}, & \text{IBCO}^+ \text{ orbiter} \end{cases}. \quad (42)$$

The ISCO<sup>+</sup> case reproduces the finding of HK, and the IBCO<sup>+</sup> case matches the findings of JS [2, 5, 6]. The appropriate values for particle 1 from Table I can be used to confirm<sup>4</sup>.

### C. Type V collisions with circular orbit plunging particles

The general formula for the CM energy of a singly source divergent collision ( $q_1 < p_c \leq q_2$ ) which occurs in the deepest part of the geometry ( $p_c = 1$ ) is given by

$$\begin{aligned} \frac{E_{\text{cm}}^2}{m_1 m_2} &= \frac{4\mu_1 l_1 \mathcal{Z}}{(1 + \cos^2 \theta)(R^2 - 1)\kappa^{1-q_1}}, \\ \mathcal{Z} &= z - \sqrt{z^2 - (R^2 - 1)(1 + \mu_2^2 + \eta_2)}, \\ z &= 2\mu_2(R - l_2\sigma_2). \end{aligned} \quad (43)$$

When particle 1 is generic ( $q_1 = 0$ ), we see the characteristic  $E_{\text{cm}} \propto (1 - a^2/M^2)^{-1/4}$  divergence.

If particle 2 is an ISCO<sup>+</sup> or IBCO<sup>+</sup> plunger, the CM energy is reduced to

$$\frac{E_{\text{cm}}^2}{m_1 m_2} = \frac{4\mu_1 l_1}{\kappa^{1-q_1}} \begin{cases} \frac{2}{\sqrt{3}(R+1)}, & \text{ISCO}^+ \\ \frac{2R - \sqrt{2}(1 + |R - \sqrt{2}|)}{R^2 - 1}, & \text{IBCO}^+ \end{cases} \text{ plunger} \quad (44)$$

When particle 1 is generic and the collision occurs at the horizon ( $R = 1$ ), the ISCO<sup>+</sup> case reproduces the finding of HK, and the IBCO<sup>+</sup> case matches the findings of JS and GP [2–5]. The appropriate values for particle 1 from Table I can be used to confirm<sup>4</sup>.

Notably, despite the factor of  $(R^2 - 1)$  in the denominator of (43), as in the ISCO<sup>+</sup> and IBCO<sup>+</sup> plunger cases (44), the CM energy of collisions is finite at the horizon. Taking the near-horizon limit  $R - 1 \ll 1$ , (43) becomes

$$\frac{E_{\text{cm}}^2}{m_1 m_2} = \frac{\mu_1 l_1 (1 + \mu_2^2 + \eta_2)}{\mu_2 (1 + l_2 \sigma_2) (1 + \cos^2 \theta) \kappa^{1-q_1}}. \quad (45)$$

Taking particle 2 to be a particle plunging from the ISCO<sup>+</sup> or IBCO<sup>+</sup> here also reproduces the results of HK and JS, respectively.

Finally, circular orbit plunging particles can source divergence in a collision only if  $q_o < p_c \leq 1$ , which by (38) occurs for  $p_o < 1/2$ . Neither ISCO<sup>+</sup> nor IBCO<sup>+</sup> particles can participate in double divergent collisions.

All previously explored high energy collisions have included ISCO<sup>+</sup> or IBCO<sup>+</sup> particles, so doubly divergent collisions have thus far gone unnoticed. A doubly divergent collision between circular orbit plunging particles of near-horizon radii

$$r_{o1} = M(1 + R_{o1}\kappa^{p_{o1}}), \quad r_{o2} = M(1 + R_{o2}\kappa^{p_{o2}}), \quad (46)$$

where  $q_{o1} = 2p_{o1} \leq q_{o2} = 2p_{o2} < p_c$ , has CM energy of the simple form

$$\frac{E_{\text{cm}}^2}{m_1 m_2} = \frac{R_{o1}}{R_{o2}\kappa^{2(p_{o2} - p_{o1})}}. \quad (47)$$

## V. NATURALNESS AND OBSERVABILITY OF HIGH ENERGY COLLISIONS

We have gone through the theoretical exercise of determining the conditions under which divergent CM energy collisions occur around near-extremal BHs, and have calculated the explicit form of the CM energy for these high energy collisions. While, experimental evidence suggest several astrophysical BHs are rotating quite rapidly [18, 19], astrophysical BHs are believed to be sub-extremal due to physical processes like accretion and back reaction [20, 21]. The CM energy grows slowly with  $\kappa$ , so the enhancement of the CM energy for rapidly rotating BHs is modest unless a very high spin cutoff is imposed.

Certainly generic particles falling towards a BH horizon are easily realized. To realize the critical particles, we can consider an accretion disk around a BH. In the case of radiatively efficient accretion flow, the accretion disk may relax into a geometrically thin, equatorial disk in which particles with radii at or above the ISCO<sup>+</sup> radius ( $r \geq r_{\text{isco}}^+$ ) travel on (quasi-)stable circular orbits, while particles interior to the ISCO<sup>+</sup> radius ( $r < r_{\text{isco}}^+$ ) plunge towards the BH while maintaining the ISCO<sup>+</sup> orbiter energy and angular momentum ( $\mu = \mu_{\text{isco}}^+$  and  $L = L_{\text{isco}}^+$ ) [22, 23]. This disk model is integral to the X-ray reflection method of measuring supermassive BH spins [24]. In this disk model, when the BH is near-extremal, the near-horizon circular orbiters can take part in Type T collisions, an plunging particles of the interior disk can take part in Type V collisions.

Thus far we have not discussed Type I collisions which require a particle to have an outward radial momentum component at the time of collision. The NHEK geometry does admit particle motion with positive radial momentum component [16, 25–27]. In principle, such particles could participate in a Type I collision, but finding the precise divergence would depend on being able to calculate the rate at which these particles scale to criticality as the near-extremal limit of orbits in the Kerr geometry,  $l\kappa^q \approx 1 - L/(2M\mu)$  for  $\kappa \ll 1$ . One way to seed a Type I collision is via a multi-scattering scenario. It has been shown that the vast majority of emission from the high energy collision of a generic particle and a circular orbiter

<sup>4</sup>For comparison to HK, our quantities  $\{\mu_1, l_1\}$  are equivalent to  $\{e_2, 1 - l/e_2\}$  of Refs. [5, 6].

For comparison to JS and GP, the near-extremal expansion in Refs. [2–4] are performed in terms of  $\epsilon = 1 - a/M \ll 1$ . Thus our small expansion parameter  $\kappa \approx \sqrt{2\epsilon}$ .

is tuned to criticality at the same rate as the orbiter (see App. B of Ref. [28]). Therefore, a daughter particle of a circular orbiter collision with  $p_r > 0$  could certainly collide with, say, another generic infalling particle.

Finally, these collisions can be observable. Despite the fact that the collisions occur in the near-horizon region, daughter particles of these high energy collisions escape to infinity where they can be observed. The near-horizon scattering processes examined to date have resulted in daughter particles with observed energy as high as the rest mass of the parent particles [2, 28–34].

### ACKNOWLEDGEMENTS

DG is grateful to Shahar Hadar helpful for discussions and detailed comments on this draft. DG is supported by a Princeton Gravity Initiative postdoctoral fellowship and by a Princeton Future Faculty in the Physical Sciences fellowship.

### Appendix A: High energy collisions on the extreme Kerr backgrounds

The extreme Kerr geometry is given by (2) with  $a = M$ . The horizon is at radius  $r = M$  and has angular velocity  $\Omega_H = 1/(2M)$ . The CM energy of particles colliding on the extreme Kerr background is given by (8) with  $a = M$ . As in the sub-extremal case, all terms in the CM energy are finite for  $r \geq M$ , with the possible exception of the term containing  $\chi$ . Taking the near-horizon limit  $r \rightarrow M$ ,

$$\chi_{\text{ext}} = \begin{cases} \frac{T_2 \hat{L}_1}{2\hat{L}_2} + \frac{T_1 \hat{L}_2}{2\hat{L}_1} + \mathcal{O}(r - M), & s_r = 1 \\ \frac{(1 - s_r)M^2 \hat{L}_1 \hat{L}_2}{(r - M)^2} + \mathcal{O}\left((r - M)^{-1}\right), & s_r \leq 0 \end{cases} \quad (\text{A1})$$

where  $\hat{L}_i = L_i - 2ME_i$ . Note the Type T and I collisions diverge faster than in the sub-extremal case (11), while the Type V collisions have the same divergence. As in the sub-extremal case, tuning the particles to criticality may change the divergence of the CM energy.

To take the near-horizon, near-critical limit, we will set

$$r = M(1 + \epsilon), \quad \epsilon \ll 1, \quad (\text{A2a})$$

$$L_i = 2M\mu_i(1 - f_i), \quad 0 \leq n_i, \quad (\text{A2b})$$

where  $f_i(n_i = 0) = \ell_i$  and  $f_i(n_i > 0) = \epsilon^{n_i}$ . The (possible) divergence of  $\chi$  (9), can be diagnosed by examining

$\tilde{P}$  and  $T$ . To leading order in the limit  $\epsilon \rightarrow 0$ ,

$$\tilde{P}_i = 2M\mu_i \begin{cases} 1 + \delta(1 - n_i), & n_i \geq 1 \\ \frac{1 + \ell_i \delta(n_i)}{\epsilon^{1-n_i}}, & 0 < n_i < 1 \end{cases}, \quad (\text{A3})$$

$$T_i = M^2 \left[ 1 + \mu_i^2 [1 + \ell_i \delta(n_i)]^2 \right] + Q_i, \quad (\text{A4})$$

where  $\delta(x)$  is the Dirac delta function. As  $\tilde{P}_i$  is non-vanishing and  $T_i$  is finite,  $R_i \propto \tilde{P}_i^2 - T_i \geq 0$  imposes no condition on  $n_i$ .

Divergent CM energy requires at least one particle satisfies  $n_i < 1$ . For singly sourced divergence of all collision Types ( $n_1 < 1 \leq n_2$ ),

$$\chi_{\text{ext}} = \tilde{P}_1 \tilde{P}_2 - s_r \tilde{P}_1^2 \sqrt{\tilde{P}_2^2 - T_2} \sim \frac{1}{\epsilon^{1-n_1}}. \quad (\text{A5})$$

For doubly sourced divergence of Type I and T collisions ( $n_1 \leq n_2 < 1$ ),

$$\chi_{\text{ext}} = (1 - s_r) \tilde{P}_1 \tilde{P}_2 \sim \frac{1}{\epsilon^{2-n_2-n_1}}. \quad (\text{A6})$$

For doubly sourced divergence of Type V collisions ( $n_1 < n_2 < 1$ ),

$$\chi_{\text{ext}} = \frac{T_2 \tilde{P}_1}{2\tilde{P}_2} \sim \frac{1}{\epsilon^{n_2-n_1}}. \quad (\text{A7})$$

### Appendix B: High energy particle collisions on NHEK and near-NHEK backgrounds

This appendix reviews the near-horizon geometry of a BH with small deviation from extremality  $\kappa \ll 1$ , i.e., the NHEK and near-NHEK metrics, then discusses collisions therein.

One obtains the near-horizon geometry of a near-extremal BH, by applying a one-parameter family of coordinate transformations [8, 25]

$$t = \frac{2MT}{\kappa^p}, \quad r = M(1 + R\kappa^p), \quad \phi = \Phi + \frac{T}{\kappa^p}, \quad (\text{B1})$$

with  $0 < p \leq 1$  to the Kerr metric (2) and taking the  $\kappa \ll 1$  limit. In this limit, the Kerr metric is  $ds^2 = ds_p^2 + \mathcal{O}(\kappa^p)$  where the leading order contribution is itself a solution to Einstein's equations. The limiting metrics are the NHEK and near-NHEK metrics which take the form

$$\frac{ds_p^2}{2M^2\Gamma} = - (R^2 - \sigma) dT^2 + \frac{dR^2}{R^2 - \sigma} + d\theta^2 + \Lambda^2 (d\Phi + R dT)^2 \quad (\text{B2})$$

where  $\Gamma = (1 + \cos^2 \theta)/2$  and  $\Lambda = 2 \sin \theta / (1 + \cos^2 \theta)$ , and where  $\sigma = \delta(1 - p)$ . The (near-)NHEK horizons are located at  $R = \sigma$ .



Timelike geodesic motion on the (near-)NHEK background can be parameterized by the particle mass  $m$ , specific energy  $\mathcal{U}$ , specific azimuthal angular momentum  $\mathcal{L}$ , and specific Carter constant  $\mathcal{Q}$ . The momentum  $P$  is given by

$$\frac{P}{m} = -\mathcal{U} dT + \bar{s}_R \frac{\sqrt{\mathbf{R}(R)}}{R^2 - \sigma} dR + \bar{s}_\theta \sqrt{\Theta(\theta)} d\theta + \mathcal{L} d\Phi \quad (\text{B3})$$

where the radial and angular potentials are

$$\Theta(\theta) = \mathcal{Q} + \left(1 - \frac{1}{\Lambda^2}\right) \mathcal{L}^2 - 2M^2\Gamma, \quad (\text{B4})$$

$$\mathbf{R}(R) = \mathcal{P}^2 - (\mathcal{Q} + \mathcal{L}^2)(R^2 - \sigma), \quad (\text{B5})$$

with  $\mathcal{P} = \mathcal{U} + \mathcal{L}R$ .

The CM energy is then given by

$$\frac{\mathcal{E}_{\text{cm}}^2}{m_1 m_2} = \frac{m_1^2 + m_2^2}{m_1 m_2} + \frac{2(X - Y)}{M^2\Gamma}, \quad (\text{B6})$$

$$X = \frac{\mathcal{P}_1 \mathcal{P}_2 - \bar{s}_{R_1} \bar{s}_{R_2} \sqrt{\mathbf{R}_1} \sqrt{\mathbf{R}_2}}{R^2 - \sigma}, \quad (\text{B7})$$

$$Y = \frac{\mathcal{L}_1 \mathcal{L}_2}{\Lambda^2} + \bar{s}_{\theta_1} \bar{s}_{\theta_2} \sqrt{\Theta_1} \sqrt{\Theta_2}. \quad (\text{B8})$$

In the near-horizon limit, the only term in the CM energy which may be divergent is that which includes  $X$ . In limit  $R \rightarrow \sigma$

$$X = \begin{cases} \frac{(\mathcal{Q}_2 + \mathcal{L}_2^2) \hat{\mathcal{U}}_1}{4 \hat{\mathcal{U}}_2} + \frac{(\mathcal{Q}_1 + \mathcal{L}_1^2) \hat{\mathcal{U}}_2}{4 \hat{\mathcal{U}}_1}, & s_R = 1 \\ -\frac{\mathcal{L}_1 \mathcal{L}_2}{2\Lambda^2} + \mathcal{O}(R - \sigma) \\ \frac{(1 - s_R) \hat{\mathcal{U}}_1 \hat{\mathcal{U}}_2}{2(1 + \sigma)(R - \sigma)^{2-\sigma}}, & s_R \leq 0 \\ +\mathcal{O}\left((R - \sigma)^{1-\sigma}\right) \end{cases} \quad (\text{B9})$$

where  $s_R \equiv \bar{s}_{R_1} \bar{s}_{R_2}$  and  $\hat{\mathcal{U}}_i \equiv \mathcal{U}_i + \sigma \mathcal{L}_i$ . The behavior of the CM energy of collisions on the (near-)NHEK background is analogous to that on the sub-extremal Kerr background (9) where Type T and I are divergent in the without any consideration of fine tuning the conserved quantities of the particles, while Type V collisions are not. The Type V collision may be divergent if the specific energy of either particle goes to zero or infinity.

The near-horizon Type V collision on the NHEK background was first discussed by Galajinsky in Ref [35], wherein it is noted the previously seen divergent near-horizon Type V collision found by BSW and others comes from calculating the CM energy in the Kerr background before taking the near-horizon near-extremal limit, while the finite one found here comes from taking the near-horizon, near-extremal limit first and then calculating the CM energy on the (near-)NHEK background. The order of limits is important as the various  $p$ -bands of the rapidly rotating BH geometry become decouple at extremality,  $\kappa = 0$ .

Nonetheless, if we consider the (near-)NHEK background in which we work to be a part of the throat of

a near-extremal BH, we can use information which descends from the Kerr geometry in the near-horizon near-extremal limit to inform us about the (near-)NHEK conserved quantities for the particles [36, 37]. Applying the coordinate transform (B1) to the Kerr momentum (4), the time and azimuthal angle components are

$$\frac{p_T}{m} = -\frac{2M\mu - L}{\kappa^p}, \quad \frac{p_\Phi}{m} = L, \quad (\text{B10})$$

where we take  $0 < p < 1$  if we are in the NHEK background and  $p = 1$  in the near-NHEK background. In the multi-scaling limit (23), the Kerr momentum connects to the (near-)NHEK momentum,

$$-\mathcal{U} = \frac{P_T}{m} = \lim_{\kappa \rightarrow 0} \frac{p_T}{m} \approx \frac{2M\mu l}{\kappa^{p-q}}, \quad (\text{B11})$$

$$\mathcal{L} = \frac{P_\Phi}{m} = \lim_{\kappa \rightarrow 0} \frac{p_\Phi}{m} \approx 2M\mu(1 - l\kappa^q). \quad (\text{B12})$$

In the multi-scaling limit, the particle's (near-)NHEK angular momentum  $\mathcal{L}$  and Kerr angular momentum  $L$  are the same; regardless of the tuning rate of the Kerr angular momentum to criticality  $q$ , the (near-)NHEK angular momentum is finite. On the other hand, in the multi-scaling limit, the (near-)NHEK specific energy  $\mathcal{U}$  becomes divergent, vanishing, or nonzero but finite according to whether the Kerr angular momentum is tuned to criticality at a rate slower, faster, or equal to the rate needed to scaling into the  $p$ -band of the throat corresponding to the (near-)NHEK background in which we are working.

When the (near-)NHEK specific energies  $\mathcal{U}_i$  are of the form (B11),  $X$  may be divergent under the same conditions as the analogous Kerr quantity (9). If  $X$  is divergent, we find divergent CM energy of the form

$$\frac{\mathcal{E}_{\text{cm}}^2}{m_1 m_2} \approx \frac{2X}{M^2\Gamma} \quad (\text{B13})$$

For singly sourced divergence of all collision Types ( $q_1 < p_c \leq q_2$ ),

$$X = \frac{2M\mu_1 l_1 \mathcal{L}_2 R}{(R^2 - \sigma)\kappa^{p-q_1}} - s_R \frac{2M|\mu_1 l_1| \sqrt{\sigma(\mathcal{Q}_2 + \mathcal{L}_2^2) - \mathcal{Q}_2 R^2}}{(R^2 - \sigma)\kappa^{p-q_1}}, \quad (\text{B14})$$

where in the NHEK ( $\sigma = 0$ ) we also require  $\mathcal{Q}_2 = 0$ . For doubly sourced divergence of Type I and T collisions ( $q_1 \leq q_2 < p_c$ ),

$$X = 8M^2(1 - s_R) \frac{\mu_1 \mu_2 l_1 l_2}{(R^2 - \sigma)\kappa^{2p-q_2-q_1}}. \quad (\text{B15})$$

For doubly sourced divergence of Type V collisions ( $q_1 < q_2 < p_c$ ),

$$X = \frac{2M^2(\mathcal{Q}_2 + \mathcal{L}_2^2)\mu_1 l_1}{\mu_2 l_2 \kappa^{q_2-q_1}}. \quad (\text{B16})$$

- [1] M. Bañados, J. Silk, and S. M. West, “Kerr Black Holes as Particle Accelerators to Arbitrarily High Energy,” *Phys. Rev. Lett.* **103** no. 11, (Sept., 2009) 111102, [arXiv:0909.0169 \[hep-ph\]](#).
- [2] T. Jacobson and T. P. Sotiriou, “Spinning Black Holes as Particle Accelerators,” *Phys. Rev. Lett.* **104** no. 2, (Jan., 2010) 021101, [arXiv:0911.3363 \[gr-qc\]](#).
- [3] A. A. Grib and Y. V. Pavlov, “On particle collisions near Kerr’s black holes,” *arXiv e-prints* (July, 2010) [arXiv:1007.3222](#), [arXiv:1007.3222 \[gr-qc\]](#).
- [4] A. A. Grib and Y. V. Pavlov, “On particle collisions in the gravitational field of the Kerr black hole,” *Astroparticle Physics* **34** no. 7, (Feb., 2011) 581–586, [arXiv:1001.0756 \[gr-qc\]](#).
- [5] T. Harada and M. Kimura, “Collision of an innermost stable circular orbit particle around a Kerr black hole,” *Phys. Rev. D* **83** no. 2, (Jan., 2011) 024002, [arXiv:1010.0962 \[gr-qc\]](#).
- [6] T. Harada and M. Kimura, “Collision of two general geodesic particles around a Kerr black hole,” *Phys. Rev. D* **83** no. 8, (Apr., 2011) 084041, [arXiv:1102.3316 \[gr-qc\]](#).
- [7] J. M. Bardeen, W. H. Press, and S. A. Teukolsky, “Rotating Black Holes: Locally Nonrotating Frames, Energy Extraction, and Scalar Synchrotron Radiation,” *ApJ* **178** (Dec., 1972) 347–370.
- [8] J. Bardeen and G. T. Horowitz, “Extreme Kerr throat geometry: A vacuum analog of  $AdS_2 \times S^2$ ,” *Phys. Rev. D* **60** no. 10, (Nov., 1999) 104030, [arXiv:hep-th/9905099 \[hep-th\]](#).
- [9] T. Harada and M. Kimura, “Black holes as particle accelerators: a brief review,” *Classical and Quantum Gravity* **31** no. 24, (Dec., 2014) 243001, [arXiv:1409.7502 \[gr-qc\]](#).
- [10] A. A. Grib and Y. V. Pavlov, “Black holes and particles with zero or negative energy,” *Theoretical and Mathematical Physics* **190** no. 2, (Feb., 2017) 268–278, [arXiv:1601.02592 \[gr-qc\]](#).
- [11] I. Bredberg, T. Hartman, W. Song, and A. Strominger, “Black hole superradiance from Kerr/CFT,” *Journal of High Energy Physics* **2010** (Apr., 2010) 19, [arXiv:0907.3477 \[hep-th\]](#).
- [12] D. E. A. Gates, S. Hadar, and A. Lupsasca, “Maximum observable blueshift from circular equatorial Kerr orbiters,” *Phys. Rev. D* **102** no. 10, (Nov., 2020) 104041, [arXiv:2009.03310 \[gr-qc\]](#).
- [13] S. Hod, “Marginally bound (critical) geodesics of rapidly rotating black holes,” *arXiv e-prints* (July, 2017) [arXiv:1707.05680](#), [arXiv:1707.05680 \[gr-qc\]](#).
- [14] L. C. Stein and N. Warburton, “Location of the last stable orbit in Kerr spacetime,” *Phys. Rev. D* **101** no. 6, (Mar., 2020) 064007, [arXiv:1912.07609 \[gr-qc\]](#).
- [15] E. Teo, “Spherical orbits around a Kerr black hole,” *General Relativity and Gravitation* **53** no. 1, (Jan., 2021) 10, [arXiv:2007.04022 \[gr-qc\]](#).
- [16] G. Compère and A. Druart, “Near-horizon geodesics of high spin black holes,” *Phys. Rev. D* **101** no. 8, (Apr., 2020) 084042, [arXiv:2001.03478 \[gr-qc\]](#).
- [17] J. Levin and G. Perez-Giz, “Homoclinic orbits around spinning black holes. I. Exact solution for the Kerr separatrix,” *Phys. Rev. D* **79** no. 12, (June, 2009) 124013, [arXiv:0811.3814 \[gr-qc\]](#).
- [18] C. S. Reynolds, “Observing black holes spin,” *Nature Astronomy* **3** (Jan., 2019) 41–47, [arXiv:1903.11704 \[astro-ph.HE\]](#).
- [19] P. A. Draghis, J. M. Miller, M. C. Brumback, A. C. Fabian, J. A. Tomsick, and A. Zoghbi, “An Extreme Black Hole in the Recurrent X-ray Transient XTE J2012+381,” [arXiv:2307.06988 \[astro-ph.HE\]](#).
- [20] K. S. Thorne, “Disk-Accretion onto a Black Hole. II. Evolution of the Hole,” *ApJ* **191** (July, 1974) 507–520.
- [21] E. Berti, V. Cardoso, L. Gualtieri, F. Pretorius, and U. Sperhake, “Comment on “Kerr Black Holes as Particle Accelerators to Arbitrarily High Energy”,” *Phys. Rev. Lett.* **103** no. 23, (Dec., 2009) 239001, [arXiv:0911.2243 \[gr-qc\]](#).
- [22] I. D. Novikov and K. S. Thorne, “Astrophysics of black holes,” in *Black Holes (Les Astres Occlus)*, pp. 343–450. Jan., 1973.
- [23] C. T. Cunningham, “The effects of redshifts and focusing on the spectrum of an accretion disk around a Kerr black hole,” *ApJ* **202** (Dec., 1975) 788–802.
- [24] L. W. Brenneman and C. S. Reynolds, “Constraining Black Hole Spin via X-Ray Spectroscopy,” *ApJ* **652** no. 2, (Dec., 2006) 1028–1043, [arXiv:astro-ph/0608502 \[astro-ph\]](#).
- [25] S. Hadar, A. P. Porfyriadis, and A. Strominger, “Gravity waves from extreme-mass-ratio plunges into Kerr black holes,” *Phys. Rev. D* **90** no. 6, (Sept., 2014) 064045, [arXiv:1403.2797 \[hep-th\]](#).
- [26] S. Hadar and A. P. Porfyriadis, “Whirling orbits around twirling black holes from conformal symmetry,” *Journal of High Energy Physics* **2017** no. 3, (Mar., 2017) 14, [arXiv:1611.09834 \[hep-th\]](#).
- [27] D. Kapec and A. Lupsasca, “Particle motion near high-spin black holes,” *Classical and Quantum Gravity* **37** no. 1, (Jan., 2020) 015006, [arXiv:1905.11406 \[hep-th\]](#).
- [28] D. E. A. Gates and S. Hadar, “Signatures of particle collisions near extreme black holes,” *arXiv e-prints* (Sept., 2023) [arXiv:2309.04572](#), [arXiv:2309.04572 \[gr-qc\]](#).
- [29] T. Piran, J. Shaham, and J. Katz, “High Efficiency of the Penrose Mechanism for Particle Collisions,” *ApJ* **196** (Mar., 1975) L107.
- [30] T. Piran and J. Shaham, “Production of gamma-ray bursts near rapid rotating accreting black holes,” *ApJ* **214** (May, 1977) 268–299.
- [31] T. Piran and J. Shaham, “Upper bounds on collisional Penrose processes near rotating black-hole horizons,” *Phys. Rev. D* **16** no. 6, (Sept., 1977) 1615–1635.
- [32] M. Bejger, T. Piran, M. Abramowicz, and F. Håkanson, “Collisional Penrose Process near the Horizon of Extreme Kerr Black Holes,” *Phys. Rev. Lett.* **109** no. 12, (Sept., 2012) 121101, [arXiv:1205.4350 \[astro-ph.HE\]](#).
- [33] E. Leiderschneider and T. Piran, “Maximal efficiency of the collisional Penrose process,” *Phys. Rev. D* **93** no. 4, (Feb., 2016) 043015, [arXiv:1510.06764 \[gr-qc\]](#).
- [34] S. Liberati, C. Pfeifer, and J. Relancio, “Exploring black holes as particle accelerators: hoop-radius, target particles and escaping conditions,” *J. Cosmology*

- Astropart. Phys. **2022** no. 5, (May, 2022) 023, [arXiv:2106.01385 \[gr-qc\]](#).
- [35] A. Galajinsky, “Near horizon geometry of extremal black holes and Banados-Silk-West effect,” *arXiv e-prints* (Jan., 2013) [arXiv:1301.1159](#), [arXiv:1301.1159 \[gr-qc\]](#).
- [36] S. E. Gralla, A. Lupsasca, and A. Strominger, “Near-horizon Kerr magnetosphere,” *Phys. Rev. D* **93** no. 10, (May, 2016) 104041, [arXiv:1602.01833 \[hep-th\]](#).
- [37] D. Gates, D. Kapec, A. Lupsasca, Y. Shi, and A. Strominger, “Polarization Whorls from M87 at the Event Horizon Telescope,” *Proceedings of the Royal Society A* **476** no. 2237, (Sep, 2020) 20190618, [arXiv:1809.09092 \[hep-th\]](#).